Effective-medium tight-binding model for silicon

K. Stokbro

Center for Atomic-Scale Materials Physics and Physics Department,
Technical University of Denmark, DK 2800 Lyngby, Denmark

N. Chetty

Department of Physics, Brookhaven National Laboratory, Upton, New York 11973

K. W. Jacobsen and J. K. Nørskov

Center for Atomic-Scale Materials Physics and Physics Department,
Technical University of Denmark, DK 2800 Lyngby, Denmark

A method for calculating the total energy of Si systems, which is based on the effective-medium-theory concept of a reference system, is presented. Instead of calculating the energy of an atom in the system of interest, a reference system is introduced where the local surroundings are similar. The energy of the reference system can be calculated self-consistently once and for all while the energy difference to the reference system can be obtained approximately. We propose to calculate it using the tight-binding linear-muffin-tin-orbital scheme with the atomic-sphere approximation (ASA) for the potential, and by using the ASA with charge-conserving spheres we are able to treat open systems without introducing empty spheres. All steps in the calculational method are *ab initio* in the sense that all quantities entering are calculated from first principles without any fitting to experiment. A complete and detailed description of the method is given together with test calculations of the energies of phonons, elastic constants, different structures, surfaces, and surface reconstructions. We compare the results to calculations using an empirical tight-binding scheme.

I. INTRODUCTION

Two parallel developments have changed our way of understanding and predicting the energetics and dynamics of condensed-matter systems over the past few years. One is the development of *ab initio* total-energy methods[1] based on density-functional theory,[2] and the local-density approximation.[3] It is now possible to calculate total energies and equilibrium configurations of systems with up to a few hundreds of atoms,[4] and in other cases it has been possible to study the molecular dynamics directly.[1,5,6] During this time, there has been a parallel development of approximate and semiempirical total-energy methods,[7-13] which has made it possible to treat the dynamics and thermal properties of systems with many thousand atoms with a reasonable accuracy.[14,15] With such methods it is now possible to treat problems in materials physics where extended defects or long range disorder are crucial for the properties that are under study.

The hope is to develop methods with the accuracy and robustness of the *ab initio* methods which can handle the larger systems on a reasonable time scale. One problem with the *ab initio* methods is the fact that the computer time scales as the cube of the number of atoms. Developments of methods where the computer time scales linearly with the size of the system have all focused on localized basis sets.[16,17] One important problem here is to construct the Hamiltonian. A natural choice would

be to use the linear-muffin-tin-orbital (LMTO) method in the tight-binding formulation,[18] but at the present time these methods usually rely on semiempirical tight-binding models constructed to fit a set of properties.

In the present paper, we introduce a very efficient and accurate method for calculating total energies for Si based on density-functional theory. The method is approximate, but computationally very efficient (two orders of magnitude faster than conventional *ab initio* methods). A set of well defined approximations are made in the total-energy expression where we rely on the variational nature of the generalized total-energy functional to compute energies reliably. Since the approximations are very systematic, we are able to test the validity of the assumptions at each stage, and therefore in a controlled way develop a hierarchy of models with various levels of approximations. All input terms are calculated theoretically, i.e., no fitting to experiment. We have earlier demonstrated the versatility of the first levels of approximations in its application to metallic Al.[19]

The method utilizes the effective-medium theory concept of an effective medium or reference system. Instead of calculating the total energy of a system of interacting Si atoms directly, we associate with each atom in the system a reference system where the energy of the atom can be calculated easily and where the surroundings of the atom in question are sufficiently similar to those of the system of interest that the energy difference can be calculated approximately. Our main approxima-

tions are to use a transferable input charge density[20] and a transferable effective potential.[21] From these approximations the energy difference can be calculated with a density-dependent pair potential and an LMTO tight-binding Hamiltonian, with all the in-going parameters determined from the transferable charge density and effective potential.

We have made extensive comparisons of the results of this method with self-consistent calculations of elastic properties, phonons, surfaces, different crystallographic phases, surface reconstructions, and adatoms on surfaces. In all cases the quality of the results is good, and we show that in the cases where the empirical tight-binding method is known to fail, the method works well.

The main result of the present paper is the scheme to calculate total energies for Si systems, which is summarized in the first part of Sec. IV. The basis of the method is the Harris functional and the effective-medium theory concept of a reference system. These aspects of the paper are discussed in Sec. II and the first part of Sec. III. In the second part of Sec. III we construct the LMTO tight-binding model from which the one-electron energy is calculated. The tests of the method are given in Sec. IV, which also includes a discussion of the relation of the present method to the empirical tight-binding method.

II. THE FIRST LEVEL OF APPROXIMATION: THE OPTIMIZED DENSITY AND HARRIS FUNCTIONAL

A. General remarks

The so-called Harris functional[22] is a good starting point for investigating the theoretical foundations of the tight-binding method[23,24] due to the non-self-consistent nature of the functional and the fact that it only depends on the input charge density. If the input density is good enough,[25] then this will give a considerable savings in computer time since only a single iteration of the Kohn-Sham equations is needed. In this work, we invoke these properties of the Harris functional to develop a model potential for Si.

B. Constructing atomiclike optimized densities

We have discussed previously[20,26] the systematic decomposition of a self-consistent total charge density into atomiclike optimized densities

$$n(\mathbf{r}) = \sum_{\mathbf{R}_\mu} \Delta n_{op}(\mathbf{r} - \mathbf{R}_\mu). \qquad (1)$$

Here, we use norm-conserving nonlocal pseudo-potentials[27,28] within a plane-wave basis[29] at an energy cutoff of 12 Ry to compute the self-consistent charge densities of bulk Si and the ideal (111) surface from which we extract the reciprocal-space components of the optimized density $\Delta n_{op}(k)$ (see Appendix A). Reverting to real space, the optimized density shown in Fig. 1 has
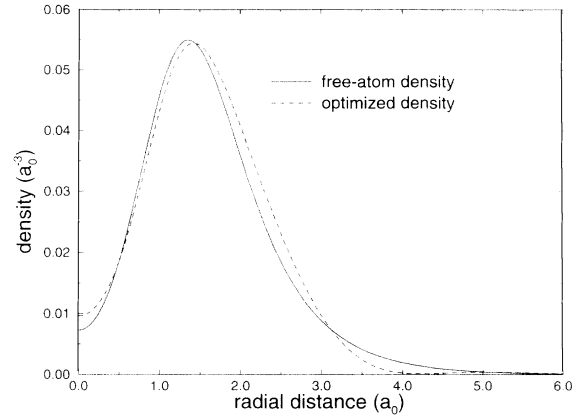
FIG. 1. The free atom density (solid) and optimized density (dashed) for Si.

the well known features of a contraction in the outer core region and a sharper attenuation of the tail with some barely discernible Friedel oscillations.[30] As noted before,[20] embedding an atom in a homogeneous electron gas at typical metallic densities produces very similar features, and this is of interest here because renormalizing the atom in this manner is the basis of the effective-medium theory of Jacobsen, Nørskov, and Puska.[12]

We have extracted reciprocal-space components of the optimized density for the other two principal surface orientations, viz. (100) and (110), and we find that to a good approximation, the components fall on the same universal curve. We will now make the assumption that $\Delta n_{op}(r)$ is indeed universal and transferable, and in the next subsection we will test this ansatz by computing the Harris functional for various different test situations and comparing with the self-consistent results.

C. Results

In order to test the accuracy of the approximations at each step in the potential construction, we will use a data base of test systems. This data base covers silicon in different crystallographic structures at the equilibrium volume, phonons, elastic constants, and surfaces. For the surfaces, we have used a supercell geometry with 12 atoms, and for all calculations we ensure an adequate sampling[31] of the Brillouin zone.

In Table I, we compare the Harris with the self-consistent results. We also include the effective-medium tight-binding (EMTB) results and those of the empirical tight-binding model of Ref. 39, which we discuss in the next section. We note that using the Harris functional with our choice of input-charge density, constructed from spherically-symmetric atomiclike densities (i.e., without bond charges), there is excellent corroboration with the self-consistent results. Other studies[32,33] using the free atom density as an input into the Harris functional have reproduced the bulk self-consistent results with a similar degree of accuracy.

EFFECTIVE-MEDIUM TIGHT-BINDING MODEL FOR SILICON

TABLE I. The self-consistent (SC), the Harris functional (H), and the effective-medium tight-binding (EMTB) results for the lattice constant a_0, bulk modulus B, and cohesive energy E_c for Si in the diamond structure. The energy relative to the diamond phase of the β tin, simple cubic, bcc, and fcc structure at the equilibrium lattice constant as obtained from the self-consistent calculation. The phonon frequencies of the transverse acoustics phonon at the X point, the transverse optical phonon at the X point, the longitudinal acoustic and optical phonon at the X point LAO(X), and the longitudinal and transverse optical phonon at the Γ point LTO(Γ). The three cubic elastic constants. The energies of the ideal principal surface orientations. In the last column (EmpTB) we show the values obtained with the empirical tight-binding model of Ref. 39.

Quantity	Units	SC	H	EMTB	EmpTB
(a) Diamond bulk					
a_0	Å	5.395	5.380	5.380	5.42
B	Mbar	0.99	0.93	0.93	1.04
E_c	eV	5.85	5.83	5.83	4.70
(b) Structures					
β tin (4.76 Å)	eV/atom	0.26	0.25	0.27	0.60
sc(2.51 Å)	eV/atom	0.41	0.41	0.43	0.73
bcc(3.03 Å)	eV/atom	0.55	0.52	0.65	1.31
fcc(3.79 Å)	eV/atom	0.56	0.54	0.77	1.32
(c) Phonons					
$\nu_{TA}(X)$	THz	4.3	4.2	4.0	5.0
$\nu_{TO}(X)$	THz	14.1	13.3	19.0	16.6
$\nu_{LOA}(X)$	THz	12.3	12.2	12.7	14.4
$\nu_{LTO}(\Gamma)$	THz	15.7	15.6	19.6	18.5
(d) Elastic constants					
C_{11}	Mbar	1.70	1.65	1.43	1.46
C_{12}	Mbar	0.72	0.62	0.90	0.78
C_{44}^0	Mbar	1.10	1.10	1.64	1.23
(e) Surfaces					
(100)	eV/atom	2.19	2.10	2.43	1.65
(110)	eV/atom	1.27	1.28	1.46	1.43
(111)	eV/atom	1.45	1.43	1.47	1.43

Our first result is that the total energies of the ideal surfaces of this semiconducting material are accurately derived from a non-self-consistent calculation. It is interesting to note that this is so despite the fact that the exact position of the surface states are known to be sensitive to the degree of self-consistency. The reason is simply that the total energy is stationary in the density while the position of the surface states are not. We therefore emphasize that the derived potential should only be used for predicting physical quantities which are stationary in the density.

III. THE SECOND LEVEL OF APPROXIMATION: THE EFFECTIVE-MEDIUM TIGHT-BINDING MODEL

A. General remarks

We will use the effective-medium construction as a basis for making further approximations. The effective-medium idea is to first calculate the total energy for a series of reference systems, and then for a given system relate each atom to a reference system, and only calculate the energy difference between the two systems. If the reference system is chosen wisely, the energy difference will be small, and can therefore be calculated approximately. To find the appropriate reference system, we will introduce the concept of a neutral sphere, defined to be a sphere around an atom for which the electron density exactly compensates the positive atomic charge. As reference system we will use silicon in the diamond structure with a lattice constant such that the neutral-sphere radius is the same in the reference system as for the atom in the original system.

In calculating this energy difference, we will utilize that the Hohenberg-Kohn density functional can be generalized to a functional $E[n, v]$ which depends on both the density n and the potential v (Refs. 12 and 23) and which is stationary with respect to independent variations of each variable. The general functional can be written as

$$E[n, v] = \sum_\alpha \epsilon_\alpha[v] - \int n(\mathbf{r})v(\mathbf{r})d\mathbf{r} + E_{el}[n] + E_{xc}[n],$$

(2)

where $\epsilon_\alpha[v]$ denotes the eigenvalues generated by solving the Kohn-Sham equation with the potential v, and where $E_{el}[n]$ and $E_{xc}[n]$ is the electrostatic and exchange-correlation energy, respectively. If the potential is restricted to be a functional of the density, the Hohenberg-

Kohn functional or the Harris functional appear as special cases.[12]

We have already used the stationary property of the density by calculating the total energy using a superposition of atom-based optimized densities. We will show that from this approximation the electrostatic and exchange-correlation energy can be transformed into a density-dependent pair-potential sum by linearizing the exchange-correlation functional.

In order to get a simple scheme for calculating the kinetic energy we will use the atomic-sphere approximation (ASA). We thereby exploit the stationary property of the the kinetic-energy functional with respect to variations in the potential by substituting the full potential with the spherically-averaged potential within each neutral sphere. Furthermore, we have recently shown[21] that the spherically-averaged potential of the reference system is very similar to that of the real system, and since the kinetic-energy functional is stationary in the potential it is a good approximation to substitute the spherically-averaged potential within each sphere with the potential of the reference system. This last approximation transforms the potential-energy contribution to the kinetic-energy difference into a sum of density-dependent pair potentials.

The remaining term is the one-electron energy which we calculate using an LMTO tight-binding Hamiltonian. Since the only potential appearing in the problem is now that of the reference system, we can precalculate the potential parameters and, by constructing an interpolation formula for the structure constants, we obtain a simple density-dependent two-center tight-binding Hamiltonian.

We have now given a brief description of the main approximations used in the construction of the EMTB model. In the following, we give a more detailed account of the construction.

B. The diamond reference system and the neutral-sphere radius

In the original effective-medium theory of Ref. 7, each atom is viewed as embedded in the electron density from the neighboring atoms and, when averaged, this density provides an effective medium in the form of a homogeneous electron gas. The role of the homogeneous electron gas is to provide a reference system in which the atoms have similar chemical surroundings as in the original system. In order to obtain the total energy, corrections due to the nonsmoothness of the charge density have to be included; however, these corrections are small and can be calculated approximately. We will use the effective-medium construction and calculate the total energy E as

$$E = \sum_i e^{\text{ref}}(s_i) + \left[E - \sum_i e^{\text{ref}}(s_i) \right], \qquad (3)$$

where we use the neutral-sphere radius s_i of each atom to define the reference system and $e^{\text{ref}}(s)$ is the energy of the reference system with neutral-sphere radius s. Note that

since the electron density is constructed using Eq. (1), the choice of identical neutral spheres in the two systems is equivalent to the choice of identical embedding density used in Ref. 7.

For silicon in the pseudopotential scheme the neutral sphere contains four electrons, and from Eq. (1) we obtain the equation

$$4 = \sum_j \Gamma(d_{ij}, s_i) , \qquad (4)$$

where Γ is the electron-density contribution from atom j to a sphere at site i of radius s_i,

$$\Gamma(d, s) = \int_s d\mathbf{r} \Delta n_{\text{op}}(|\mathbf{r} - \mathbf{d}|). \qquad (5)$$

We solve Eq. (4) iteratively for the neutral-sphere radius, using a cutoff distance of $r_c = 11.67a_0$ to terminate the sum (we thereby include five neighbor shells in the equilibrium diamond lattice). For this lattice, the nearest-neighbor distance is $d_0 = 4.40a_0$ and we obtain a neutral-sphere radius of $s_0 = 2.72a_0$. In Fig. 2 we show the neutral-sphere radius of the diamond structure as a function of the nearest-neighbor distance. For comparison, we also show the Wigner-Seitz radius of the diamond lattice and the $2^{1/3}$ smaller Wigner-Seitz radius of a diamond lattice embedded in a bcc lattice with empty spheres. We see that in the diamond structure the neutral-sphere radius is substantially smaller than the Wigner-Seitz radius. This difference is due to the large regions in the diamond lattice which contain almost no charge and therefore are not included in the neutral sphere. In a more close-packed system like the fcc system the neutral-sphere radius is more or less equal to the Wigner-Seitz (WS) radius.

As a reference system we will use the diamond structure, and the energy correction therefore vanishes for a diamond lattice or an isolated atom, since the latter can be regarded as a diamond lattice with an infinite lattice constant. So by construction the EMTB will give the
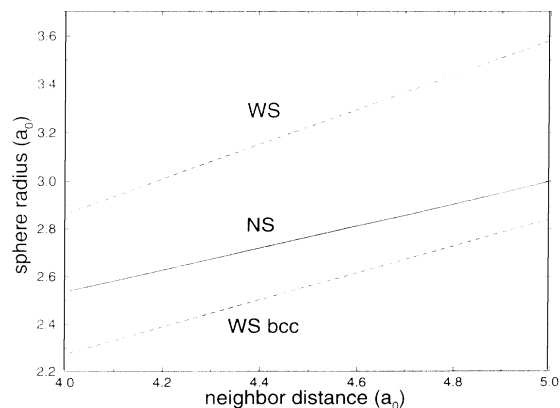
FIG. 2. The neutral-sphere radius(solid) for silicon in the diamond lattice as a function of the nearest-neighbor distance. The dashed lines show the Wigner-Seitz radius of the diamond lattice, and of an inscribed bcc lattice.

correct cohesive energy, bulk modulus, and equilibrium lattice constant for the diamond structure.

In order to calculate the energy difference to the reference system, we divide the total energy into two terms: the kinetic energy (T) and the sum of the electrostatic and exchange-correlation energy (G),

$$E = \sum_i e^{\text{ref}}(s_i) + \left[T - \sum_i t^{\text{ref}}(s_i) \right]$$
$$+ \left[G - \sum_i g^{\text{ref}}(s_i) \right], \qquad (6)$$
$$E = \sum_i e^{\text{ref}}(s_i) + \Delta T + \Delta G.$$

So far we have just rearranged the terms in the total energy. The first approximation we make is to calculate the kinetic energy in the ASA. The quality of this approximation depends on how well the full potential can be approximated by a superposition of spherically-averaged potentials within atomic spheres. Traditionally, the ASA is made using space-filling spheres on the ground that with this choice integrals over space may be mapped into integrals over the spheres — the integration of a constant function will therefore be correct in the ASA. However, since the density enters all integrals, we will use neutral spheres, making the spheres charge conserving instead of volume conserving — the integration of a constant function times the density is correct. This choice seems more physical since we thereby obtain that both the ASA density and the full density contains the correct number of electrons. When the ASA is made with volume conserving spheres the ASA density is usually fixed to include the correct number of electrons, however, the corresponding full density, which is accessible in the LMTO method,[18] will then not contain the correct number of electrons.

In Fig. 3 we show the full self-consistent potential of sil-
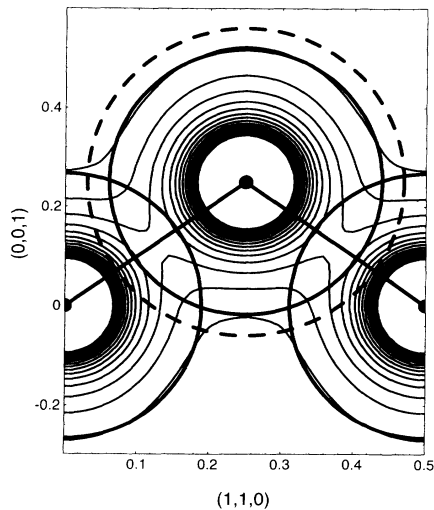
FIG. 3. The self-consistent potential of silicon in the diamond lattice projected onto the $(1\bar{1}0)$ plane. The solid circle show the radius of the neutral-sphere radius, while the dashed circle show the Wigner-Seitz radius.

icon in a (110) diamond plane, together with the neutral-sphere radius (solid circle) and Wigner-Seitz radius (dotted circle). It is clear from the figure that the overlap region of the WS spheres penetrates far into the spherically symmetric parts of the potential, which would lead to a poor approximation of the full potential. The overlap region of the neutral spheres, on the other hand, very accurately sample only the asymmetric part of the potential and since the potentials are superimposed the approximation is enhanced in this region. We will use the ASA with neutral spheres, and because we thereby obtain an accurate approximation for the full potential we may avoid the traditional usage of empty spheres in ASA calculations for open structures.

We have recently shown that with our choice of reference system the ASA potential of a general system is almost identical to the potential of the reference system,[21] so that we may at each site substitute the potential within the atomic sphere with the reference potential. Furthermore, due to the variational properties of the energy functional, this only leads to errors in the total energy of second order in the potential difference $(v - v^{\text{ref}})$. We then have for the kinetic-energy difference

$$\Delta T \approx \sum_{\alpha \in \text{occ}} \epsilon_\alpha [\bar{v}^{\text{ref}}] - \sum_i e_{1\text{el}}(s_i)$$
$$- \sum_i \int_{s_i} \bar{v}^{\text{ref}}(r, s_i)[n(\mathbf{r}) - n^{\text{ref}}(\mathbf{r})] d\mathbf{r} \qquad (7)$$
$$\equiv \Delta E_{1\text{el}} + \Delta V,$$

where $\bar{v}^{\text{ref}}$ is the spherically-averaged potential of the reference system, and $e_{1\text{el}}(s)$ is the one-electron energy of the reference system with neutral-sphere radius s.

Let us now summarize the total binding-energy expression in the form used in the effective-medium theory of Ref. 12. The total binding energy is given by

$$E = E_c + \Delta E_{\text{as}} + \Delta E_{1\text{el}}$$

$$(8)$$

$$= \sum_i e^{\text{ref}}(s_i) + [\Delta G + \Delta V] + \Delta E_{1\text{el}},$$

where E_c, ΔE_{as}, and $\Delta E_{1\text{el}}$ are called the cohesive function, atomic-sphere correction, and one-electron correction, respectively.

The first term, the cohesive function, is the energy of the reference system, which we parametrize using the interpolation formula[34]

$$E_c(s) = E_0(1 + x)e^{-x}, \quad x = \lambda(s - s_0). \qquad (9)$$

In this equation, $E_0 = -5.83$, is the cohesive energy of the equilibrium diamond lattice and the parameter, $\lambda = 2.047$, is determined by the bulk modulus of the diamond lattice.

The second term, the atomic-sphere correction, can be viewed as a correction to an ASA calculation of the electrostatic and exchange-correlation energy. To see this we use the definition of the effective potential $\bar{v}^{\text{ref}} = \frac{\partial \bar{g}^{\text{ref}}}{\partial n}$, where $\bar{g}^{\text{ref}}$ is the ASA electrostatic and exchange-correlation energy of the reference system. We can now

TABLE II. The effective-medium components of the Harris functional results of Table I. The second column show the lattice constant of the structure and the displacement used for the frozen phonon and elastic deformation calculations.

Quantity		H	E_c	ΔE_{as}			ΔE_{1el}
				ΔG_{el}	ΔG_{xc}	ΔV	
β tin	(4.76 Å)	0.25	0.00	-1.39	-0.80	0.67	1.78
sc	(2.51 Å)	0.41	0.01	-0.99	-0.64	0.37	1.67
bcc	(3.03 Å)	0.52	0.01	-1.94	-1.13	0.96	2.62
fcc	(3.79 Å)	0.54	0.00	-1.75	-1.16	0.61	2.84
TA(X)	(0.04)	0.025	0.002	-0.053	-0.022	0.035	0.062
TO(X)	(0.02)	0.059	0.001	-0.062	0.023	0.14	-0.044
LOA(X)	(0.02)	0.099	0.029	-0.050	0.007	0.096	0.017
LTO(Γ)	(-0.01)	0.145	0.002	-0.133	0.031	0.277	-0.032
LTO(Γ)	(0.01)	0.099	0.001	-0.068	0.025	0.150	-0.009
C_{11}	(0.06)	0.0361	0.0229	-0.0060	-0.0034	0.0051	0.0174
$2(C_{11} - C_{12})$	(0.06)	0.0450	0.0005	-0.0257	-0.0117	0.0170	0.0650
C_{44}^0	(0.06)	0.0241	0.0003	-0.0235	0.0050	0.0463	-0.0039
(100)		2.10	0.40	0.36	0.68	0.32	0.34
(110)		1.28	0.10	0.20	0.52	0.23	0.23
(111)		1.43	0.10	0.24	0.58	0.24	0.27

identify the $-\Delta V$ term of Eq. (8) as the first term in a Taylor expansion of the difference in the ASA electrostatic and exchange-correlation energy between the system and the reference systems ($\Delta \bar{G}$), and we therefore have $\Delta E_{as} = \Delta G - \Delta \bar{G} + O([n - n^{ref}]^2)$. We see that the atomic-sphere correction is the first order correction to a calculation where not only the kinetic energy, but also the exchange and correlation energy have been calculated within the ASA, i.e., the ASA has been used for both the potential and the density. In the next section we will show that the atomic-sphere correction can be calculated by a density-dependent pair potential.

The third term, the one-electron correction, is the energy correction due to the difference in band structure between the system and the reference system, and in Sec. III D we will calculate this term using an LMTO tight-binding model.

In Table II we show the EMTB terms for the test systems of Table I. The cohesive energy and atomic-sphere correction were extracted from a Harris functional calculation and the one-electron correction then obtained by subtracting these terms from the total energy. With this data base we may not only check the potential by calculating the total energy, but we may test the accuracy of each term in the energy separately. For now we will just note that the contribution from the cohesive function to the energy of the equilibrium structures is very small, indicating that it is the minimum of this function that determines the equilibrium volumes. Since the cohesive function depends only on the neutral-sphere radius, this implies that all the equilibrium structures have almost the same neutral-sphere radius, even though the equilibrium volumes are very different.

C. Calculating the atomic-sphere correction with a density-dependent pair potential

We will now decompose the atomic-sphere correction into density-dependent pairwise interactions. The inter-

actions depend on the local density through the neutral-sphere radius s

$$E_{as} = \sum_{i,j} V(d_{ij}, s_i), \tag{10}$$

where the density-dependent pair potential is composed of three parts

$$V(d, s) = V_v(d, s) + V_{el}(d) + V_{xc}(d, s), \tag{11}$$

which originates from the ΔV term, the electrostatic energy, and the exchange-correlation energy, respectively. From Eqs. (1) and (8) we see that Eq. (10) is exact for the ΔV term and the electrostatic energy, with the density-dependent pair potentials given by

$$V_v(d, s) = \int_s \bar{v}^{ref}(r, s) \, \Delta n_{op}(|\mathbf{r} - \mathbf{d}|)d\mathbf{r}, \tag{12}$$

$$V_{el}(d) = \frac{1}{2} \int \left(\frac{-Z}{r} + \int \frac{\Delta n_{op}(r')}{|\mathbf{r} - \mathbf{r}'|} d\mathbf{r}' \right)$$
$$\times \left[\Delta n_{op}(|\mathbf{r} - \mathbf{d}|) - Z\delta(|\mathbf{r} - \mathbf{d}|) \right] d\mathbf{r}$$
$$+ \int \left(v_l(r) - \frac{-Z}{r} \right) \Delta n_{op}(|\mathbf{r} - \mathbf{d}|)d\mathbf{r}. \tag{13}$$

In the last equation Z is the ionic pseudocharge, and the last term correct for the difference between the ionic potential and the pseudopotential. Note that we only include the local part of the pseudopotential v_l, since the nonlocal part is canceled between the electrostatic energy and the potential part of the kinetic energy.

To calculate the exchange-correlation energy we use the local-density functional of Ref. 35, and from the decomposition of the density we have

$$E_{xc} = \sum_i \int \Delta n_{op}(|\mathbf{r} - \mathbf{R}_i|) \, \mathcal{E}_{xc}(n(\mathbf{r})) \, d\mathbf{r}. \tag{14}$$

In order to approximate this term with a density-dependent pair-potential sum we will have to divide the

TABLE III. The table shows the value of the ΔG_{xc} term for the structures of Table II. The column denoted H is the value of the term calculated using the Harris functional, the column denoted EMTB is the result obtained using the approximations of the EMTB model, and in the third column a parameter has been allowed in order to scale all the energies.

Quantity		H	ΔG_{xc} EMTB	$\times 1.28$
β tin	(4.76 Å)	-0.80	-0.62	-0.80
sc	(2.51 Å)	-0.64	-0.48	-0.62
bcc	(3.03 Å)	-1.13	-0.90	-1.16
fcc	(3.79 Å)	-1.16	-0.94	-1.21
TA(X)	(0.04)	-0.022	-0.015	-0.020
TO(X)	(0.02)	0.023	0.016	0.020
LOA(X)	(0.02)	0.007	0.001	0.002
LTO(Γ)	(-0.01)	0.031	0.023	0.029
LTO(Γ)	(0.01)	0.025	0.018	0.023
C_{11}	(0.06)	-0.0034	-0.0025	-0.003 39
$2(C_{11} - C_{12})$	(0.06)	-0.0117	-0.0082	-0.0105
C_{44}^0	(0.06)	0.0050	0.0030	0.0038
(100)		0.68	0.31	0.40
(110)		0.52	0.25	0.32
(111)		0.58	0.26	0.33

exchange-correlation functional into contributions from each atom, which may be obtained by using a linear expansion for the exchange-correlation functional. We have chosen to linearize the exchange-correlation functional around the spherically-averaged density of the reference system, $\bar{n}(r, s)$, and thereby obtain the density-dependent pair potential

$$V_{xc}(d, s) = \int \Delta n_{op}(r) \frac{\partial \mathcal{E}_{xc}}{\partial n}(\bar{n}(r, s)) \Delta n_{op}(|\mathbf{r} - \mathbf{d}|) d\mathbf{r}.$$

(15)

In Table III we compare the exchange-correlation part
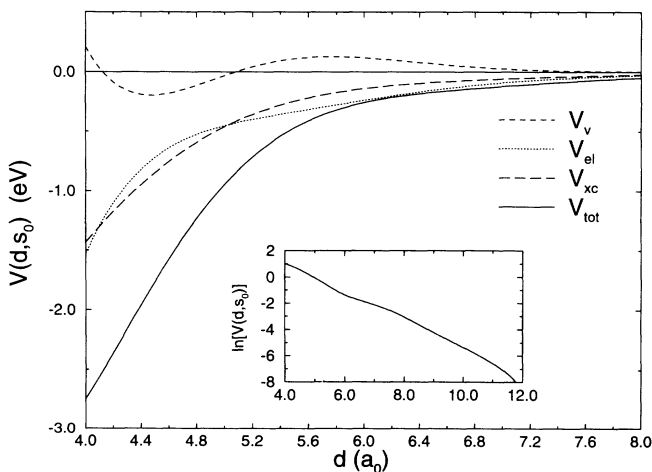
FIG. 4. The density-dependent pair potential, and its three components, used for calculating the atomic-sphere correction as function of distance, with the neutral-sphere radius fixed at s_0. The inlet shows the logarithm of the density-dependent pair potential.
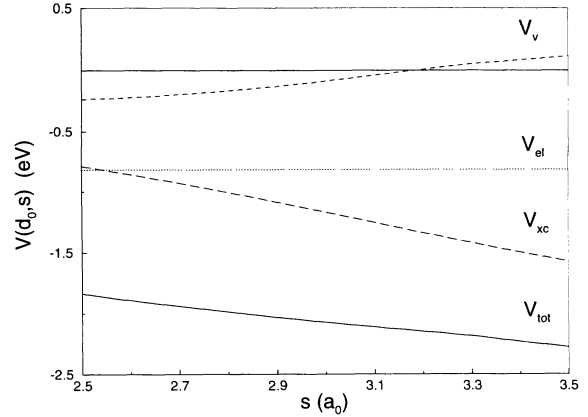
FIG. 5. The density-dependent pair potential as a function of the neutral-sphere radius (s), with the distance fixed at d_0.

of the atomic-sphere correction calculated using this density-dependent pair potential to an exact evaluation of the exchange-correlation integral. We see that the correction generally is underestimated by 20%. This suggests that a better approximation might be obtained if the exchange-correlation functional is linearized at a lower density than the mean density, possibly because it varies more rapidly in the low density regime. We have not addressed this problem further, being satisfied with the fact that when a factor is allowed for rescaling the density-dependent pair potential we obtain a good description of the exchange-correlation energy, as shown in the third column of Table III.

We conclude this section by showing in Fig. 4 the distance dependence of the density-dependent pair potentials, and in Fig. 5 the dependence upon the neutral-sphere radius. We see that the distance dependence of the sum is nearly exponential even though the distance dependence of the individual components is not. The dependence upon the neutral-sphere radius is dominated by the contribution from the exchange-correlation part, which approximately scales as s^2, originating from the scaling of the mean density in the reference system.

D. Calculating the one-electron correction with an LMTO tight-binding model

Returning to the expression for the total energy, Eq. (8), we have already given expressions for the first two terms and need only to calculate the one-electron correction to obtain the total energy. This is the most time consuming step in a total-energy calculation since it involves the diagonalization of a Hamiltonian. The key number in this context is the number of basis functions (N) because the computer time used in conventional diagonalization schemes scales as $O(N^3)$. In the Car-Parrinello method the scaling is $O(NM^2)$ where M is the system size. However, the prefactor is large such that this method generally is two orders of magnitude slower than tight-binding methods. A plane-wave basis

set is in this respect not very efficient, since many plane-waves are needed in order to get a good description of the regions around the atomic positions where the electron density varies rapidly. Instead, we will use a partial wave method in which the basis functions are augmented with the the local solution of the Schrödinger equation around each atom, and therefore only a small basis set is needed.

However, the partial waves depend on the energy at which the Schrödinger equation is solved, and the Hamiltonian thereby becomes energy dependent. This problem is solved very elegantly in the linearized band structure methods where an energy independent basis set is obtained by linearizing the solutions of the Schrödinger equation around a fixed energy ϵ_ν. We will use the LMTO method,[18] and with these basis functions, called LMTO's, the eigenvalues become correct to first order in the difference with the energy ϵ_ν, and a systematic expansion exists for the higher order corrections. For now we will only consider the first order approximation, and we may then neglect the overlap of the orbitals, since the overlap enters as a higher order correction.

Since we use the ASA for calculating the kinetic energy the first order LMTO Hamiltonian becomes especially simple. It separates into potential parameters Δ^α, C^α determined from the potentials in the atomic spheres, and structure constants S^α which only depend on the positions of the atomic spheres[18]

$$H^\alpha_{iL,jL'} = C^\alpha_{il}\delta_{iL,jL'} + (\Delta^\alpha_{il})^{1/2} S^\alpha_{iL,jL'}(\Delta^\alpha_{jl'})^{1/2} , \quad (16)$$

where we use the notation $L = lm$ for the angular-momentum quantum numbers, and we will use an sp^3 basis set.

The index α in Eq. (16) denotes the representation we use for the LMTO's. The conventional LMTO's are the $\alpha = 0$ representation in which the structure constants have simple two-center forms

$$S^0_{iL',iL} = 0 , \quad S^0_{\{ss\sigma,sp\sigma,pp\sigma,pp\pi\}}$$
$$= \{-2x^{-1}, 2\sqrt{3}x^{-2}, 12x^{-3}, -6x^{-3}\} , \quad (17)$$

where x is a relative distance measure given by

$$x = d_{ij}/w_{ij} , \quad w_{ij} = s_0\frac{d[(s_i + s_j)/2]}{d_0}. \quad (18)$$

In this equation $d[s]$ is a function that returns the nearest-neighbor distance in the diamond lattice with neutral-sphere radius s, such that we have the same relative distance $x_0 = d_0/s_0$, for all diamond lattices. Note that the LMTO Hamiltonian will not depend on the choice of w as defined in Eq. (18), since the w dependence of the structure constants is canceled by a similar term in the potential parameters.

It is possible to shift to a representation where the neighboring sites, through a screening "charge" α, are used to localize the structure constants.[18] The structure constants now depend on the local structure through a matrix equation (the LMTO Dysons equation)

$$S^\alpha_{iL,jL'} = S^0_{iL,jL'} + \sum_{kL''} S^0_{iL,kL''}\alpha_{l''}S^\alpha_{kL'',jL'}. \quad (19)$$

We use the screening constants $\alpha_{s,p} = \{0.3072, 0.0316\}$ which are related to the sp-screening parameters of Ref. 18 through a scaling of $(1.07)(2l + 1)$.

With this choice of screening constants we have calculated the structure constants for all the test systems of Table I using the LMTO Dysons equation, which involves inverting a 200×200 matrix. In Fig. 6 we show the Slater-Koster components[36] of each structure matrix, as a function of the relative distance measure(x) defined in Eq. (18). It is surprising how well the structure constants for such different surroundings as surfaces, phonons, and different crystal structures, all fall on the same curves. In Ref. 18 interpolation formulas for the structure constants of close packed structures were found by using a relative distance measure obtained by scaling the distances with the Wigner-Seitz radius. The neutral-sphere provides a natural measure, which makes it possible to extend this idea to more open structures and surfaces.

With our choice of relative distance measure we may now use the data base to construct interpolation formulas and thereby obtain a simple and fast scheme for calculating the structure constants of a general system. For the $ss\sigma$ and $pp\pi$ elements we only need to include nearest-neighbor elements, while the $sp\sigma$ and $pp\sigma$ elements are longer range, and we therefore have to include second-nearest-neighbor elements. For the interpolation we have used the functional form

$$\tilde{S}^\alpha(x) = f(x) - f(x_c) - (x - x_c)f'(x_c),$$
$$(20)$$
$$f(x) = A[1 + \lambda(x - 1)]e^{-\lambda x},$$

where the first equation ensure that the structure constants go continuous differentiable to zero at the cutoff x_c. The relative distance measure, x, is defined in Eq. (18) and A, λ are parameters to be determined from
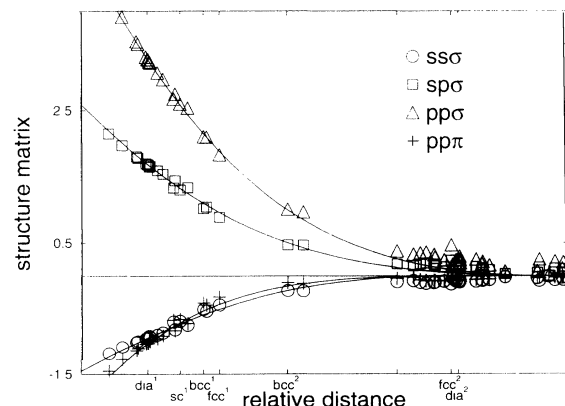
FIG. 6. The crosses show the Slater-Koster components of the structure constants for the structures in Table I as a function of the relative distance measure, x, defined in Eq. (18). The structure constants were calculated using Eq. (19). The tick marks on the horizontal axis indicate the relative distance in the diamond, simple cubic, fcc, and bcc structure. The solid lines show the value of the structure constant as obtained from the interpolation formula of Eq. (20).

the data base. We fix the parameter A from the nearest-neighbor structure constant of the diamond lattice, and determine λ by a least-squares fit to the nearest-neighbor data points of Fig. 6. The resulting approximations are shown as solid lines in Fig. 6, and the values of the parameters are given in Table IV.

The on-site elements of the screened structure matrixes are nonzero. We have from Eq. (19)

$$\sigma^\alpha_{iL,iL'} = \sum_{kL''} S^0_{iL,kL''}\alpha_{l''}\tilde{S}^\alpha_{kL'',iL'}, \quad (21)$$

where σ^α is the on-site element calculated using the approximate structure matrix $\tilde{S}^\alpha$. For the diamond structure the on-site element is diagonal and we have $\sigma^\alpha_{s,p}(\text{diamond}) = \{1.71, 1.46\}$, while it will contain off-diagonal components in a general system. However, the use of the approximate off-site structure matrixes $(\tilde{S}^\alpha)$ in Eq. (21) gives a significant error for these components, i.e., the off-diagonal components of σ_α are nonsymmetric and generally too large. We will therefore use the following approximation for the on-site structure matrix

$$\tilde{S}^\alpha_{iL,iL'} = \frac{1}{4}[\sigma^\alpha_{iL,iL'} + \sigma^\alpha_{iL',iL} + 2\sigma^\alpha_{iL,iL'}(\text{diamond})], \quad (22)$$

which is a simple average of the symmetrized value of σ^α between the system and the reference system.

We now return to the calculation of the potential parameters. These are given by the solutions at the linearization energy ϵ_ν of the radial Schrödinger equation within each atomic sphere.[38] Since we get the potential from the reference system, we only have to calculate the potential parameters for the reference system once and for all, and then use the neutral-sphere radius to find the potential parameters for a general system. In Figs. 7 and 8, we show the value of the potential parameters as a function of the neutral-sphere radius of the reference system. For each system we have chosen ϵ_ν at the center of gravity of the occupied bands. These data are accurately approximated by the interpolation formulas

$$\tilde{\Delta}^\alpha_s(s) = \Delta^\alpha_s(s_0)e^{-1.130(s-s_0)}, \quad (23)$$

$$\tilde{\Delta}^\alpha_p(s) = \Delta^\alpha_p(s_0)e^{-0.978(s-s_0)},$$

$$\tilde{C}_p(s) - \tilde{C}_s(s) = 4.67 + [C^\alpha_p(s_0)$$

$$-C^\alpha_s(s_0) - 4.67]e^{-0.76(s-s_0)},$$

TABLE IV. The value of the parameters in Eq. (20). The parameter x_c determines the range of the Hamiltonian, which for the $ss\sigma$ and $pp\pi$ element is nearest neighbor in the diamond lattice, while it is second nearest neighbor for the $sp\sigma$ and $pp\sigma$ element. The $S^\alpha(d_0/s_0)$ is the structure constants of the equilibrium diamond lattice as obtained from the LMTO Dysons equation, while λ is obtained from a least squares fit to the data points of Fig. 6.

Quantity	$ss\sigma$	$sp\sigma$	$pp\sigma$	$pp\pi$
x_c	2.60	2.95	2.95	2.60
$S^\alpha(d_0/s_0)$	-0.938	1.690	3.279	-1.025
λ	2.40	2.85	2.76	4.10
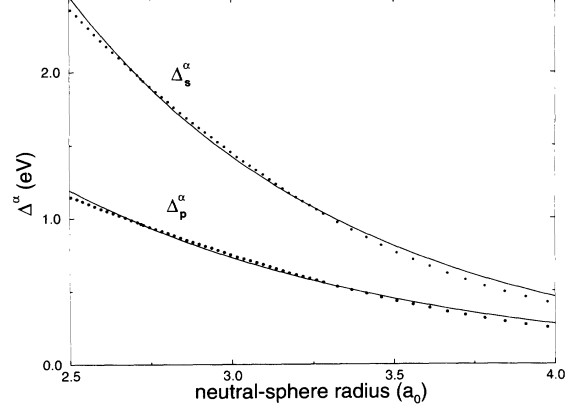
FIG. 7. The dots show the calculated potential parameters Δ^α for the diamond reference system; the solid line is the approximation obtained with the interpolation formulas of Eq. (24).

where $\Delta^\alpha_s(s_0), \Delta^\alpha_p(s_0), C^\alpha_s(s_0)$, and $C^\alpha_p(s_0)$ (unit eV) are the potential parameters in the equilibrium diamond lattice listed in Table V, and s is the neutral sphere (unit a_0). In Figs. 7 and 8 the interpolation formulas for the potential parameters are shown as solid lines.

We have now constructed the LMTO tight-binding Hamiltonian directly from the data of the ab initio plane-wave calculation. However, due to the small basis set and the incomplete description of the interstitial region the calculated band structure for the equilibrium diamond structure does not agree completely with that of the plane-wave calculation shown in Fig. 9 [self-consistent (SC)]. We find the occupied band to be 15% too wide and the band gap at the Γ point to be too small. In order to improve the Hamiltonian, we have made a least-squares fit of the potential parameters to the three lowest eigenstates at the Γ point and the two lowest at the X point. By this procedure we include the effect of the neglected orbitals in an indirect fashion. The resulting potential parameters are shown in the second row of Ta-
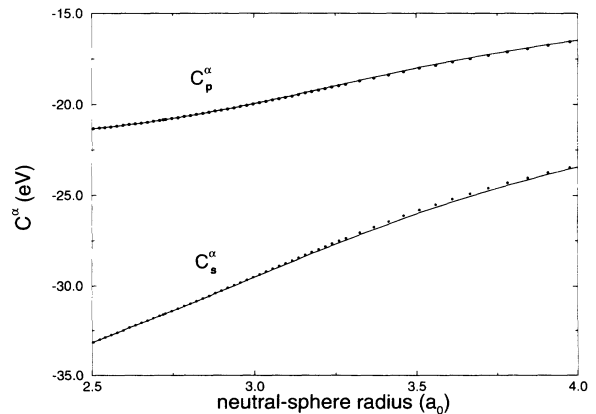
FIG. 8. The dots show the potential parameters C^α, and the solid line is the approximation obtained with the interpolation formulas of Eq. (24).

TABLE V. The LMTO potential parameters for the equilibrium diamond lattice. The values in the first row are obtained by solving the radial Schrödinger equation within the atomic sphere, the values in the second row are obtained by a least squares fit to the band structure of silicon.

Quantity	$C_p^\alpha(s_0) - C_s^\alpha(s_0)$	$\Delta_s^\alpha(s_0)$	$\Delta_p^\alpha(s_0)$
Calculated	10.73	1.954	0.959
Fitted	8.26	1.954	0.738

ble V, and we see that $\Delta_s^\alpha(s_0)$ is unchanged while both $\Delta_p^\alpha(s_0)$ and $C_p^\alpha(s_0) - C_s^\alpha(s_0)$ have been rescaled with a factor 0.77. The corresponding band structure is shown in Fig. 9 (EMTB), and we now have a good description of the occupied parts of the bands, and the band gap at the Γ point.

We are now ready to calculate the one-electron correction (ΔE_{1el}) of Eq. (8). Instead of calculating the band energy we will calculate the bond energy,[37] because we thereby remove any first order dependencies on the on-site elements

$$E_{1el} = \sum_{k \in occ} \epsilon_k - \sum_i N_i \mathcal{E}_i. \qquad (24)$$

In this equation N_i is the site projected occupation and $\mathcal{E}_i$ the site projected on-site element. The bond energy depends only weakly on the shift in the average on-site elements. For instance, for the three principal surfaces, the largest shift in the average on-site element is at the (100) surface, where it is 0.84 eV higher than in the bulk. Such a shift lowers the bond energy 0.19 eV compared to a calculation where the average on-site element is fixed at the bulk value. We have chosen to fix the average on-site element to be zero, $\mathcal{E}_i = 0$, since by this approximation the second term in Eq. (24) vanishes, and this greatly
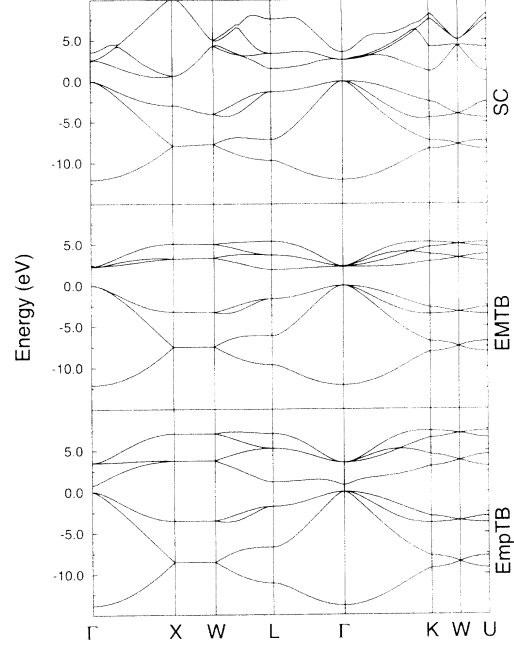
FIG. 9. The figure show the band structure of silicon calculated with three different methods. Starting from the top the calculations are self-consistent plane-wave calculation (SC), the EMTB model, and the empirical tight-binding model (EmpTB) of Ref. 39.

simplifies the calculation of forces. Due to this approximation the total energy for the surfaces will be a little too high with the EMTB model.

In Table VI we show the one-electron correction obtained with this scheme compared to the value of the plane-wave Harris functional calculation. The second column shows the the result when we use the calculated po-

TABLE VI. The table shows the value of ΔE_{1el} terms for the structures of Table II. The column denoted H is the value of the term calculated using the Harris functional, the column denoted EMTB (calc) is the result obtained using the approximations of the EMTB model, and in the third column [EMTB(fit)] the potential parameter has been obtained by fitting to the band structure. The last column (EmpTB) shows the values obtained with the empirical tight-binding model of Ref. 39.

Quantity		ΔE_{1el}			
		H	EMTB(calc)	EMTB(fit)	EmpTB
β tin	(4.76 Å)	1.78	1.82	1.76	0.38
sc	(2.51 Å)	1.67	1.70	1.62	0.81
bcc	(3.03 Å)	2.62	2.60	2.76	0.29
fcc	(3.79 Å)	2.84	2.89	3.10	0.44
TA(X)	(0.04)	0.062	0.066	0.058	0.057
TO(X)	(0.02)	-0.044	0.034	0.033	0.049
LOA(X)	(0.02)	0.017	0.027	0.020	0.062
LTO(Γ)	(-0.01)	-0.032	0.047	0.051	0.1081
LTO(Γ)	(0.01)	-0.009	0.061	0.056	0.1233
C_{11}	(0.06)	0.0174	0.0184	0.0161	0.0137
$2(C_{11} - C_{12})$	(0.06)	0.0650	0.0604	0.0525	0.0422
C_{44}^0	(0.06)	-0.0039	0.0091	0.0116	0.0168
(100)		0.34	0.89	0.94	1.15
(110)		0.23	0.57	0.58	1.23
(111)		0.27	0.53	0.55	1.23

tential parameters (first row of Table V), while the third column shows the result when we use the potential parameters obtained by fitting the band structure (second row of Table V). For all test systems the accuracy of both models is acceptable when compared with the value of the total energy of Table II. We have chosen to use potential parameters fitted to the band structure, since we then at the same time get a good description of the total energies and the band structure. In the next section we will first sum up the ingredients of the EMTB, and then compare it to empirical tight-binding schemes by applying both models to various test systems.

IV. APPLICATIONS

A. The EMTB potential

An EMTB calculation starts with loading precalculated values for the functions $\Gamma(d,s), V(d,s)$ defined in Eqs. (5) and (11), and the atomic-sphere, $e_{as}^{ref}(s)$, and one-electron energy term, $e_{1el}^{ref}(s)$, of the reference system. Next we calculate the neutral-sphere radius of each atom, s_i, from Eq. (4). The total energy is given by

$$E = \sum_i e_c(s_i) + E_{as} - \sum_i e_{as}(s_i) + E_{1el} - \sum_i e_{1el}(s_i).$$
(25)

The cohesive function $e_c(s)$ is defined in Eq. (9), and the atomic-sphere energy E_{as} defined in Eq. (10). The one-electron energy is calculated from the Hamiltonian

$$\tilde{H}_{iL,jL'}^\alpha = \tilde{C}_{il}^\alpha(s_i)\delta_{iL,jL'}$$
$$+(\tilde{\Delta}_l^\alpha(s_i))^{1/2}\tilde{S}_{L,L'}^\alpha(x_{ij})(\tilde{\Delta}_{l'}^\alpha(s_j))^{1/2},$$
(26)

where the off-site structure constants are given by the interpolation formula in Eq. (20) with the parameters of Table IV, and the relative distance measure (x) defined in Eq. (18). The on-site elements are given by Eqs. (22,21,17), using the screening $\alpha_{s,p} = \{0.3072, 0.0316\}$. The potential parameters are calculated from the interpolation formulas of Eq. (24) with the constraint that the average on-site element at each site is zero ($\mathcal{E}_i = 0$), and using the values in the last row of Table V for $\Delta^\alpha(s_0), C^\alpha(s_0)$. With this model we have calculated the total energy for the test systems of Table I and the corresponding results are shown in the third column.

B. Empirical tight-binding (EmpTB)

In a conventional empirical tight-binding scheme the energy function consists of an attractive band structure term describing the bonding in the system and a repulsive pair potential usually interpreted as arising from the overlap interaction. For the comparison we will use the tight-binding model of Goodwin et al.,[39] with a fixed cutoff as in Ref. 40, and in the following we will denote this model EmpTB. The EmpTB is based on the nearest-

neighbor tight-binding model of Harrison,[41] in which the strength of the hopping integrals is obtained by fitting the band structure, and the level splitting is taken to be identical to that of the atom. Harrison assumed a universal decay of the pair potential and hopping integrals, such that the only parameter remaining to be determined is the strength of the pair potential, which was fixed to give the correct equilibrium lattice constant. The resulting model gives an excellent description of the elastic properties of silicon in the diamond structure; however, the model fails to predict the energies of different silicon phases. Goodwin et al. made the model transferable to other structures by introducing a scaling of the hopping integrals, and adjusting the level splitting. Their model has four adjustable parameters which were fixed to give the cohesive energy and bulk modulus of the diamond and fcc structure. This scheme has proven very successful for describing systems[40] far from the structures where the tight-binding parameters were fitted, and currently most empirical tight-binding schemes use a similar functional form.

The last column in Table I shows the total energies of the test systems obtained with the EmpTB. We see that the elastic properties are described very well by the EmpTB, while the total energies of the structures and surfaces are not too accurate. However, note that the energy of the crystal structures were calculated at the equilibrium volume as obtained from the self-consistent calculation (in Fig. 10 we show the full phase diagram).
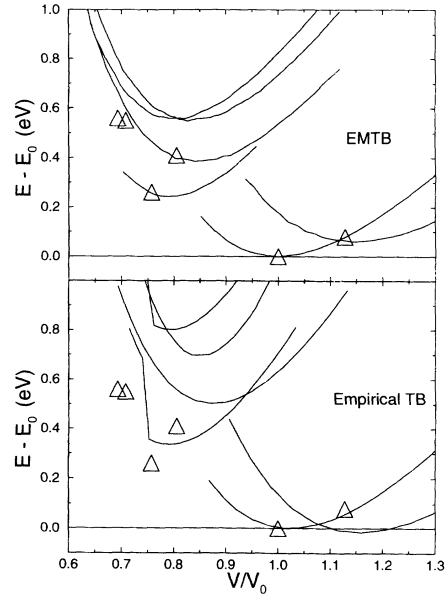
FIG. 10. The triangles in both figures show the energies of the diamond, clathrate II, β-tin, simple cubic, bcc, and fcc structure, in that order, at their respective equilibrium volumes, calculated self-consistently. The energy of the clathrate II structure is from Ref. 42. The solid lines in the upper figure show the energies of the structures calculated using the EMTB model, while the energies in the lower figure were calculated using the empirical tight-binding model of Ref. 39. The cusps on the curves in the lower figures are caused by second-nearest neighbors entering within the cutoff distance.

C. Comparison between the EMTB and EmpTB model

In Table VII we show for the two models the hopping integrals and sp level splitting in the equilibrium diamond lattice. For the EMTB we show the scaled parameters, and for the EmpTB we have included the value of $\epsilon_p - \epsilon_s$ used in Ref. 41. In Fig. 9 we show the band structure of the two models compared to a self-consistent calculation. For the EMTB model the description of the occupied bands is excellent. In the EmpTB model the description is reasonable, with the largest error for the lowest state at the Γ point. Also, the band gap at the Γ point is too small in the EmpTB model; this is of importance when the model is used together with the O(N) method of Refs. 16 and 17, where a large band gap is needed in order to make the scheme efficient.

The difference between the two tight-binding models becomes apparent when we look at the distance dependence of the matrix elements. In the EMTB the distance dependence is divided into two parts, scaling of the potential parameters and the structure matrix. When we have a uniform compression, without a structural change, only the potential parameters change. These scale approximately as $(s_0/s)^3$, which is similar to the scaling of Ref. 41. When there is a structural change the scaling should be stronger, and this scaling enters through the structure constants. In the EmpTB these two basic scalings are mixed into one function.

In the last column of Table VI we show the value of the one-electron correction as obtained when the EmpTB is used to describe the one-electron energy for the system and reference system. Clearly the EmpTB does not describe the one-electron correction, with largest discrepancies for surfaces and structural energies. For these systems we have found crystal field terms to be important, i.e., off-diagonal on-site elements and shifts of the level spacings. Such effects are not included in the EmpTB, but enter in the EMTB through Eq. (21).

Besides the one-electron term there is a pair-potential term in both models. However, the EMTB pair potential is negative, while the EmpTB pair potential is positive. The EmpTB pair potential can therefore not only describe the electrostatic and exchange-correlation energy, but must include some terms from the kinetic energy. In the work of Harrison[41] the pair potential is viewed as an overlap interaction, i.e., it is mainly due to the one-electron energy.

In the EMTB there is an additional term, the cohesive function. The fact that this term is not equal to the sum of the reference pair-potential and one-electron energies, illustrates the idea behind the reference system: Because the reference system is chosen for a given atom so that the environment of the atom is similar to the environment in the real system it is possible to calculate the energy difference with a rather crude tight-binding model. The largest error is in the shift of the average on-site term of the Hamiltonian, but since the potentials are identical in the system and reference system this error for the system is canceled by a similar error in the one-electron energy of the reference system, and the correct binding energy is then obtained through the cohesive function.

In the next section, we will calculate the phase diagram for silicon and in Secs. IV E and IV F we will investigate some of the reconstructions of the (100) and (111) surfaces.

D. Phase diagram

In Fig. 10 we show the total energies versus volume for the diamond, clathrate II,[42] β-tin, simple cubic, bcc, and fcc phases of silicon calculated with the EMTB and EmpTB schemes. The EMTB potential gives a good description of the cohesive energy and the equilibrium volume for all the phases investigated, while the EmpTB predicts the correct energy ordering of all the phases, excluding the clathrate II structure which is lower than the diamond structure, but the equilibrium volumes are shifted. The small cutoff of the interactions in the EmpTB model becomes visible for the β-tin and fcc phase, i.e., second-nearest neighbors enter within the cutoff range. In the EMTB scheme we also use a fixed cutoff, however in this case we use a relative distance measure which is scale invariant, and this ensures that for a given structure we include the same number of neighbors independent of the lattice constant. For the EMTB model we have found crystal field effects to give an important contribution to the structural energies. For instance, in the fcc phase $\epsilon_p - \epsilon_s = 5.39$ eV compared to $\epsilon_p - \epsilon_s = 5.87$ eV in the diamond phase.

E. The (100) surface

There has been a large effort to understand the different reconstructions of the (100) surface, involving a wide range of experimental and theoretical tools since different reconstructions occur at different length scales. However, the reconstructions are so complex that there are still a lot of unsolved problems, especially for systems involving too few atoms in order for elasticity theory to be correct,

TABLE VII. The tight-binding parameters of the equilibrium silicon structure for the EMTB and the empirical tight-binding (EmpTB) scheme of Ref. 39. For the EMTB we show the rescaled parameters. In Ref. 39 the four hopping integrals for the EmpTB were taken from Ref. 41 and the level splitting fitted to the fcc — diamond energy difference. The number in parentheses is the value of Ref. 41.

Model	$H_{ss\sigma}$	$H_{sp\sigma}$	$H_{pp\sigma}$	$H_{pp\pi}$	$\epsilon_p - \epsilon_s$
EMTB	-1.79	1.99	2.37	-0.74	5.87
EmpTB	-1.82	1.96	3.06	-0.87	8.295(6.83)

and too many atoms to be feasible for plane-wave methods.

There is a general consensus that the main building block for all the reconstructions is the buckled 1×2 dimer reconstruction. This structure was first predicted by Chadi[43] from a tight-binding calculation, and lately also self-consistent plane-wave calculations[44,45] have found this structure to be lower in energy than a symmetric dimer reconstruction. So for a potential to give a detailed description of the various reconstructions on the (100) surface, it should at least predict the correct 1×2 dimer reconstruction.

In Table VIII we show the result of a relaxation of the (100) 1×1 and 2×1 reconstructions using the EMTB and EmpTB compared to the results of self-consistent plane-wave calculations. For both models the description of the structure of the 1×2 reconstruction is good, but the EMTB gives a too high relaxation energy, while the relaxation energy of the EmpTB is far too small. For the EMTB the driving force for the reconstruction is the atomic-sphere correction, and not the one-electron correction. The atomic-sphere correction always drives the system to more close packed structures, and in this case that can be done without an increase in the one-electron energy. Both models predict an outward relaxation of the

1×1 cell, while the self-consistent calculation predicts an inward relaxation.

F. The (111) surface

Also the (111) surface has many interesting reconstructions, the most famous being the 7×7 Tagayanagi reconstruction.[46] This reconstruction is built from adatom geometries where the adatoms sit on top sites, and studies using self-consistent plane-wave calculations have confirmed the stability of adatoms in top site positions.[47,48] For a potential to predict the correct reconstructions of the (111) surface it therefore has to describe these adatom geometries properly.

In Table VIII we show the result of a relaxation of the (111) 1×1 surface, and of the top and hollow site adatom geometries in a $\sqrt{3}\times\sqrt{3}$ cell. The self-consistent numbers are from two different references; the top site geometry were calculated in Ref. 48 with a ten layer slab and a 12 Ry cutoff. In the other reference[47] the energy of the adatom in both the top and hollow positions where calculated but with an eight layer slab using a 6 Ry cutoff. We see that both tight-binding models predict the top site to be more stable than the hollow site geometry; how-

TABLE VIII. Energies and structures of the (100) and (111) surface obtained from self-consistent, EMTB, and EmpTB calculations. The γ denote the surface energy per 1×1 cell, and $\Delta\gamma$ the surface energy relative to the ideal 1×1 cell. For the relaxed 1×1 geometries we show the relative relaxation of the first layer atoms, Δ_{12}. For the (100) 1×2 structure we show the dimer bond length, r_d, and buckling angle, θ. For the (111) $\sqrt{3}\times\sqrt{3}$ T_4 structure we show the relaxation toward the adatom axis (dotted line in Fig. 11), δr, and the relaxation in the vertical direction, δz. The atom numbers refer to Fig. 11.

Geometry	Quantity	Unit	SC	EMTB	EmpTB
The (100) Surface					
Ideal 1×1	γ	eV	2.19	2.43	1.65
Relaxed 1×1	$\Delta\gamma$	eV	-0.03^{a}	-0.02	-0.03
	Δ_{12}	%	-5.1^{a}	4.8	4.5
Relaxed 1×2	$\Delta\gamma$	eV	-0.85^{b}	-1.04	-0.39
	θ	Degree	$(16^{0})^{b}$	19^{0}	15^{0}
	r_d	a_0	4.28^{b}	4.47	4.62
The (111) Surface					
Ideal 1×1	γ	eV	1.45	1.47	1.43
Relaxed 1×1	$\Delta\gamma$	eV	-0.06^{c} (-0.17^{d})	-0.01	-0.02
	Δ_{12}	%	-27^{c}	-7	3
$\sqrt{3}\times\sqrt{3}\ T_4$	$\Delta\gamma$	eV	-0.27^{c} (-0.28^{d})	-0.27	-0.04
	r_d	a_0	5.01^{c} (4.70^{d})	4.89	4.95
	$\delta r(2)$	a_0	-0.35^{c} (-0.28^{d})	-0.35	-0.23
	$\delta z(2)$	a_0	0.03^{c} (-0.15^{d})	0.10	0.12
	$\delta z(3a)$	a_0	-0.71^{c} (-0.74^{d})	-0.65	-0.57
	$\delta z(3b)$	a_0	0.38^{c} (0.18^{d})	0.18	0.21
	$\delta z(4a)$	a_0	-0.54^{c} (-0.48^{d})	-0.58	-0.62
	$\delta z(4b)$	a_0	0.23^{c} (0.11^{d})	0.06	0.12
	$\delta r(5)$	a_0	0.10^{c}	0.09	0.13
	$\delta z(5)$	a_0	0.01^{c}	0.03	-0.04
$\sqrt{3}\times\sqrt{3}\ H_3$	$\Delta\gamma$	eV	-0.17^{d}	-0.13	-0.02

[a]Reference 50.
[b]Reference 45.
[c]Reference 48.
[d]Reference 47.
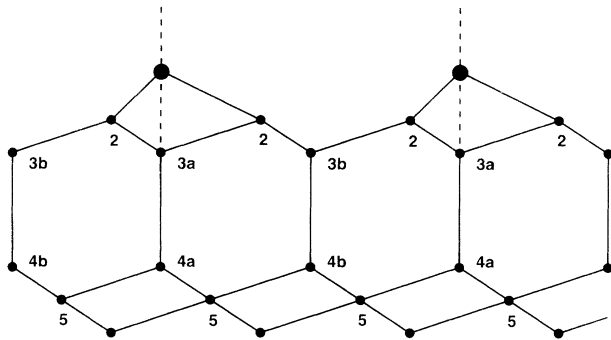
FIG. 11. The geometry of the top site adatom on the (111) surface.

ever, the formation energies obtained with the EmpTB are far too small, while the EMTB is in excellent agreement with the data of Ref. 48. The formation energy obtained with the empirical tight-binding scheme is too low to stabilize the adatom, and therefore additional parameters have to be introduced in order to describe the 7×7 reconstruction.[49] In Fig. 11 we show the geometry of the adatom in the top position, and in Table VIII we compare the relaxed coordinates.

V. SUMMARY AND CONCLUSIONS

In the present paper, we have presented a method for total-energy calculations for Si systems. We have discussed in detail the hierarchy of approximations behind the present formulation. Starting from a fully self-consistent solution of the Kohn-Sham equations the first level of approximation is to use the Harris functional with transferable, optimized densities centered at each atomic position deduced from independent self-consistent calculations for different bulk and surface structures. At this level the errors introduced compared to the fully self-consistent calculations are very small.

The next level of approximation involves the introduction of a reference system. We have shown that choosing a reference system with the same neutral-sphere radius (or average electron density) as in the real system gives one-electron potentials and potential parameters for the LMTO Hamiltonian that can be transferred from the reference system to the real system with very little error.

The energy difference between the reference system and the real system can be calculated from a difference between a density-dependent pair-potential sum in the real and the reference system and a one-electron energy difference. The former describes to a very good approximation the difference in the electrostatic, exchange correlation, and part of the kinetic energy. The one-electron energy difference taking care of the rest of the energy difference is evaluated using an LMTO tight-binding Hamiltonian.

The results of the method are very encouraging. The computational effort is similar to empirical tight-binding methods (for 150 atoms the diagonalization of the Hamiltonian takes 95% of the time, and only the last 5% is spent on the energy and force calculations), but the results seem to be better. The time consuming part of the calculation is the diagonalization of the LMTO Hamiltonian and for this part the proposed "order N" methods can be used,[16,17] since the band gap at the Γ point is well described.

APPENDIX A: PARAMETRIZATION OF THE OPTIMIZED DENSITY

We have found the optimized density to be well approximated by the functional form

$$\Delta n_{op}(k) = \Delta n_{atom}(k) + a_1 k^2 (k - a_2)(k - a_3)$$
$$\times \exp(a_4 k - a_5 k^2), \qquad (A1)$$

where $a_1 = 0.078, a_2 = 2.584, a_3 = 1.465, a_4 = 1.969, a_5 = 0.962$, and n_{atom} is the atomic density.

[1] R. Car and M. Parrinello, Phys. Rev. Lett. **55**, 2471 (1985).

[2] P. Hohenberg and W. Kohn, Phys. Rev. **136**, 3864 (1964); W. Kohn and L.J. Sham, *ibid.* **140**, A1133 (1965).

[3] For a review, see, e.g., *Theory of the Inhomogeneous Electron Gas*, edited by S. Lundqvist and N.H. March (Plenum Press, New York, 1983).

[4] I. Stich, M.C. Payne, R.D. King-Smith, J-S. Lin, and L.J. Clarke, Phys. Rev. Lett. **68**, 1351 (1992); K.D. Brommer, M. Needels, B.E. Larson, and J.D. Joannopoulos, *ibid.* **68**, 1355 (1992).

[5] A. De Vita, I. Stich, M.J. Gillan, M.C. Payne, and L.J.

Clarke, Phys. Rev. Lett. **71**, 1276 (1993).

[6] P. Margl, K. Schwartz, and P.E. Blöchl, J. Chem. Phys. (to be published).

[7] J.K. Nørskov and N.D. Lang, Phys. Rev. B **21**, 2131 (1980); J.K. Nørskov, *ibid.* **26**, 2875 (1982).

[8] M.J. Stott and E. Zaremba, Phys. Rev. B **22**, 1564 (1980).

[9] M.S. Daw and M.I. Baskes, Phys. Rev. Lett. **50**, 1285 (1983).

[10] M.W. Finnis and J.E. Sinclair, Philos. Mag. A **50**, 45 (1984).

[11] F. Ercolessi, E. Tosatti, and M. Parrinello,

Phys. Rev. Lett. **57** , 719 (1986).

[12] K.W. Jacobsen, J.K. Nørskov, and M.J. Puska, Phys. Rev. B **35**, 7423 (1987).

[13] S.B. Sinnott, M.S. Stave, T.J. Raeker, and A.E. DePristo, Phys. Rev. B **44**, 8927 (1991).

[14] O.H. Nielsen, J.P. Sethna, P. Stoltze, K.W. Jacobsen, and J.K. Nørskov, Europhys. Lett. **26**, 51 (1994).

[15] W.D. Luedtke and U. Landman, Comp. Mater. Sci. **1**, 1 (1992).

[16] M.S. Daw, Phys. Rev. B **47**, 10 895 (1993).

[17] P.-X. Li, R.W. Nunes, and D. Vanderbildt, Phys. Rev. B **47**, 10 891 (1993).

[18] O.K. Andersen and O. Jepsen, Phys. Rev. Lett. **53**, 2571 (1984). A more detailed description of the LMTO method can be found in O.K. Andersen, O. Jepsen, and M. Sob, in *Electronic Bandstructure and its Applications*, edited by M. Yussouff, Springer Lecture Notes (Springer-Verlag, Berlin, 1987).

[19] N. Chetty, K. Stokbro, K.W. Jacobsen, and J.K. Nørskov, Phys. Rev. B **46**, 3798 (1992); K. Stokbro, N. Chetty, K.W. Jacobsen, and J.K. Nørskov, *Proceedings of the 15th Tanigushi Symposium* (Springer, New York, 1993).

[20] N. Chetty, K.W. Jacobsen, and J.K. Nørskov, J. Phys. Condens. Matter **3**, 5437 (1991).

[21] K. Stokbro, N. Chetty, K.W. Jacobsen, and J.K. Nørskov, J. Phys. Condens. Matter **6**, 5415 (1994).

[22] J. Harris, Phys. Rev. B **31**, 1770 (1985).

[23] W.M.C. Foulkes and R. Haydock, Phys. Rev. B **39**, 12 520 (1989).

[24] O.F. Sankey and D.J. Niklewski, Phys. Rev. B **40**, 3979 (1989).

[25] M.W. Finnis, J. Phys. Condens. Matter **2**, 331 (1990).

[26] I.J. Robertson, M.C. Payne, and V. Heine, J. Phys. Condens. Matter **3**, 8351 (1991).

[27] E.L. Shirley, D.C. Allan, R.M. Martin, and J.D. Joannopoulous, Phys. Rev. B **40**, 3652 (1989).

[28] D. Vanderbilt, Phys. Rev. B **32**, 8412 (1985).

[29] J. Ihm, A. Zunger, and M.L. Cohen, J. Phys. C **12**, 3792 (1979).

[30] M.J. Puska, R.M. Nieminen, and M. Manninen, Phys. Rev. B **24**, 3037 (1981).

[31] H.J. Monkhorst and J.D. Pack, Phys. Rev. B **13**, 5188 (1976).

[32] A.J. Read and R.J. Needs, J. Phys. Condens. Matter **1**, 7565 (1989).

[33] H.M. Polatoglou and M. Methfessel, Phys. Rev B **37**, 10 403 (1988).

[34] J.H. Rose, J.R. Schmidt, F. Guinea, and J. Ferrante, Phys. Rev. B **29**, 2963 (1984).

[35] D.M. Ceperley and B.J. Alder, Phys. Rev. Lett. **45**, 566 (1980); J. Perdew and A. Zunger, Phys. Rev. B **23**, 5048 (1981).

[36] J.C. Slater and G.F. Koster, Phys. Rev. **94**, 1498 (1954).

[37] A.P. Sutton, M.W. Finnis, D.G. Pettifor, and Y. Ohta, J. Phys. C **21**, 35 (1988).

[38] *Muffin Tin Orbitals and Electronic Structure*, edited by H.L. Skriver (Springer-Verlag, Berlin, 1984).

[39] L. Goodwin, A.J. Skinner, and D.G. Pettifor, Europhys. Lett. **9**, 701 (1989).

[40] C.Z. Wang, C.T. Chan, and K.M. Ho, Phys. Rev. B **45**, 12 227 (1992).

[41] W.A. Harrison, Phys. Rev. B **27**, 3592 (1983).

[42] The Clathrate(34) structure is a supercell geometry consisting of 34 atoms all with coordination 4. This structure has been proposed as a new Si phase by G.B. Adams, M. O'Keefle, A.A. Demkov, O.F. Sankey, and Yin-Min Huang, Phys. Rev. B **49**, 4048 (1994), who also made us aware of the failure of the EmpTB model for this structure.

[43] D.J. Chadi, Phys. Rev. Lett. **43**, 43 (1979).

[44] N. Roberts and R.J. Needs, Surf. Sci. **236**, 112 (1990).

[45] J. Dabrowski and M. Scheffler, Appl. Surf. Sci. **56**, 15 (1992).

[46] K. Takayanagi, Y. Tanishiro, M. Takahashi, and S. Takahashi, J. Vac. Sci. Technol. A **3**, 1502 (1985).

[47] J.E. Northrup, Phys. Rev. Lett. **57**, 154 (1986). Note that this calculation was performed using a smaller unit cell than ours, and with a 6 Ry plane-wave cutoff and k-point sampling.

[48] R.D. Meade and D. Vanderbildt, Phys. Rev. B **40**, 3905 (1989). The authors have not calculated the total energy of the ideal (111) surface, so in order to obtain energies relative to the ideal surface we use the total energy from our own self-consistent calculation of the clean (111) surface.

[49] D.J. Chadi, Phys. Rev. B **30**, 4470 (1984).

[50] M.T. Yin and M.L. Cohen, Phys. Rev. B **24**, 2303 (1981).